Scientific Reports
https://doi.org/10.1038/s41598-026-41795-7
Article in Press

Electron bunch optimization in laser wakefield acceleration through temporally asymmetric pulse shaping in ionization injection regime

Received: 24 September 2025
Accepted: 23 February 2026
Published online: 25 March 2026
Cite this article as: Ravina , Kim S., Gupta D.N. *et al.* Electron bunch optimization in laser wakefield acceleration through temporally asymmetric pulse shaping in ionization injection regime. *Sci Rep* (2026). https://doi.org/10.1038/s41598-026-41795-7

Ravina, Suho Kim, Devki Nandan Gupta & Hyyong Suk

Electron bunch optimization in laser wakefield acceleration through temporally asymmetric pulse shaping in ionization injection regime

Ravina[1], **Suho Kim**[2], **Devki Nandan Gupta**[1,†], **and Hyyong Suk**[2,*]

[1]Department of Physics and Astrophysics, University of Delhi, Delhi 110 007, India
[2]Department of Physics and Photon Science, Gwangju Institute of Science and Technology, Gwangju 61005, South Korea
[†]Corresponding author: dngupta@physics.du.ac.in
[*]Corresponding author: hysuk@gist.ac.kr

ABSTRACT

In the ionization injection regime of laser wakefield acceleration (LWFA), the control and optimization of electron bunches is a major concern. We address this by demonstrating the generation of tunable electron bunches in LWFA using temporally asymmetric laser pulses in the ionization injection regime. The introduction of pulse asymmetry modifies the wakefield structure, which affects the accelerating field and electron trapping in the ionization injection regime. Our 2D PIC simulations show that fast trailing edge asymmetry of the laser pulse produces narrow electron bunches with improved energies, whereas slow trailing edge asymmetry favors prolonged injection and yields broader bunches with higher charge. These results reveal that the temporal shape of the driving laser pulse serves as a control parameter for tailoring the charge, duration, and quality of the injected electron beam. This approach offers a versatile pathway for tunable electron bunch generation in LWFA without requiring changes in plasma density or gas composition. This paves the way for the development of compact, high-brightness electron sources for advanced accelerator and radiation applications.

Introduction

Laser wakefield acceleration (LWFA) is an advanced technique for generating high-energy electron beams. It has garnered significant interest due to its potential to revolutionize particle accelerators[1–6]. Unlike conventional accelerators, which rely on large-scale systems and high-powered radio frequency cavities, LWFA exploits the electric fields generated by intense laser pulses propagating through the plasma to accelerate electrons to relativistic speeds. This method promises to produce high-energy electron beams at much smaller scales, making it a compelling alternative for next-generation accelerators[7–10].

In the context of LWFA, various electron injection schemes have been developed to improve the generation of high-quality electron beams[11–18]. Downramp injection is one approach to control the electron injection process in laser wakefield acceleration[11]. By creating a controlled plasma density gradient, this scheme improves the quality, charge, and stability of the accelerated electron bunches. The second is the ionization injection mechanism, where a high-intensity laser pulse propagates through a gas mixture consisting primarily of a low atomic number (Z) gas with small amount of high Z gas, ionizing inner shell electrons of high Z gas, right inside the wakefield. These free electrons can be controlled by optimizing the properties of the laser pulse[13,14,19]. Each scheme aims to control the injection process, which is crucial for obtaining stable and optimized electron bunches with desirable properties such as minimal energy spread and narrow bunch.

In LWFA, the performance of good-quality electron bunch generation is closely associated with the properties of the driving laser pulse, where key factors such as the shape, duration, and intensity of the pulse play a critical role in the acceleration process[20–23]. Traditionally, ionization injection has been limited by the uniformity of the laser pulse, which typically results in the injection of electrons over a wide range of plasma regions and at varying phases of the wakefield, leading to inferior quality of electron bunches[24]. To address this limitation, the temporal shaping of the laser pulse may be employed to enhance the ionization injection process by improving the resulting electron bunch characteristics, and hence offer a promising solution. These pulses, characterized by a rapid rise time followed by a slower decay or vice versa, have been shown to create a more controlled injection[25,26]. The sharp increase in the pulse intensity helps to concentrate the injection of electrons into a specific region of the plasma, optimizing the phase of the plasma wave in which the electrons are injected. This targeted injection improves the quality of the electron bunch, resulting in optimized charge and more stable electron bunches.

This study investigates the role of temporally asymmetric laser pulses in the enhancement of the ionization injection mechanism in LWFA. With an advance in our understanding of how temporally asymmetric pulses can be used to optimize the electron bunch characteristics, such as charge, energy spread, and bunch length, this work aims to contribute to ongoing efforts to make LWFA a viable technology for a wide range of scientific applications. By carefully shaping the laser pulse[27], we can effectively control and enhance the characteristics of the electron bunches in the ionization injection regime of LWFA. A systematic analysis of the electron bunch properties has been carried out through particle-in-cell (PIC) simulations. The results obtained from the two-dimensional (2D) PIC simulations have been thoroughly analyzed and presented graphically, accompanied by a comprehensive theoretical interpretation. Also, the quasi-three-dimensional (3D) PIC simulation results are provided in the Supplementary Information as additional support for the conclusions. The ability to generate optimized and high-quality electron bunches in a compact, cost-effective system could revolutionize fields such as high-energy physics, medical imaging, and material science, offering a more efficient and accessible means of achieving the high-energy beams essential for cutting-edge research[28–30].

Results

2D-PIC simulations were performed (see Methods) to investigate the influence of laser pulse shape on electron bunch generation in the ionization injection regime of LWFA. In addition, quasi-3D PIC simulations (see Supplementary Information) were conducted to validate and confirm the reliability of the observed trends. We consider a temporally asymmetric laser pulse for plasma interaction. The temporal shape of the pulse is considered either fast trailing or slow trailing . Considering a linearly polarized temporally asymmetric laser pulse with vector potential $\mathbf{A(t)} = \hat{x}A_0G(t)$, where $G(t)$ is the temporal envelope function of the asymmetric pulse. We define this function as $G(t) = e^{-t^2/t^2_{r,f}}$, where t_r is the characteristic time scale of the rising edge of the laser pulse, and t_f is the characteristic time scale of the trailing edge of the laser pulse. The electric field of the laser pulse can be given by $\mathbf{E(t)} = -\partial\mathbf{A}(t)/\partial t$. Here, we define a pulse shape parameter, $\alpha = t_f/t_r$. The pulse is symmetric for $\alpha = 1.0$ and pulse becomes temporally asymmetric for $\alpha > 1$, $\alpha < 1$.
Figure 1 illustrates how the asymmetry parameter α alters the temporal envelope of the laser electric field, impacting its interaction with the plasma. A symmetric pulse (with $\alpha = 1.0$) rises and falls uniformly, offering a standard wake excitation. The slow trailing pulse ($\alpha = 2.0$) leads to weaker initial plasma excitation and delayed wake formation, while the fast trailing pulse ($\alpha = 0.5$) that generates a stronger initial ponderomotive force and more effective early wake excitation. This shape is particularly advantageous for ionization injection, allowing for early trapping and extended acceleration, which enhances the overall energy gain of the injected electrons.

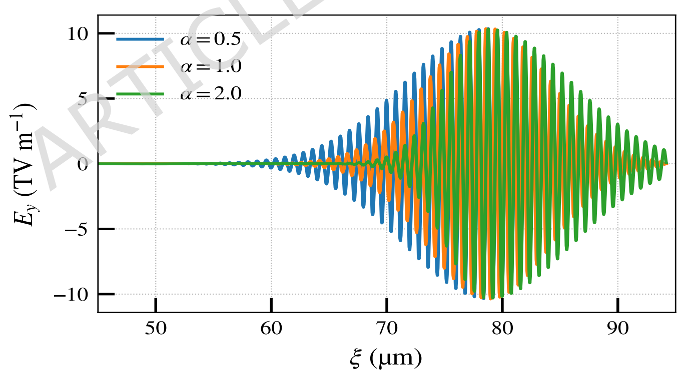

Figure 1. Electric field of the Gaussian pulses with different pulse shapes ($\alpha = 1.0, \alpha = 2.0, \alpha = 0.5$). Each plot shows a time-domain electric field distribution. The peak field remains similar, but the temporal spread changes with α, resulting in asymmetric pulses. The y-axis (Electric Field in TV/m) remains consistent across all subplots, allowing direct comparison of pulse shape.

The results presented in Fig. 2 are interpreted within the framework of LWFA in ionization injection regime, where a temporally asymmetric laser pulse propagates through a mixed gas target, typically consisting of a low Z background (e.g. hydrogen) and a high Z dopant (e.g. nitrogen). The intense, asymmetric laser electric field profile enhances field ionization of inner-shell electrons from the high Z species at specific wakefield phases. These freshly ionized electrons are born within the accelerating phase of the plasma wave and can be promptly trapped and accelerated by ionization-induced injection. To observe the influence of temporal pulse asymmetry, the pulse shape is varied using different α, while keeping the full-width at half-maximum (FWHM) of the laser pulse constant. The asymmetric pulse facilitates more efficient injection of electrons via ionization from the nitrogen dopant and allows electrons to experience longer acceleration lengths. The asymmetric pulse with $\alpha = 0.5$

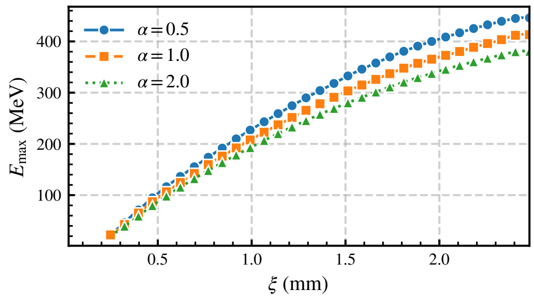

Figure 2. 2D PIC simulation results showing maximum electron energy as a function of propagation length (ξ) for laser pulses with different temporal asymmetry parameters ($\alpha = 0.5, 1.0, 2.0$). The laser has normalized vector potential $a_0 = 2.65$, spot size $r_0 = 10\ \mu$m, full-width at half-maximum (FWHM) pulse duration $\tau_{\mathrm{FWHM}} = 30$ fs, and central wavelength $\lambda = 0.8\ \mu$m. It propagates in the z-direction through a pre-ionized hydrogen plasma with an electron density of $n_0 = 5 \times 10^{18}$ cm^{-3}, doped with 0.5% nitrogen to facilitate ionization injection.

consistently yields higher maximum electron energies, as evidenced by the steeper slopes in the energy versus the propagation length (ξ) (see Fig. 2). In this case, the pulse rises more slowly, injecting fewer electrons and showing less beam loading. Therefore, the electrons can gain higher energies during acceleration. In contrast, pulses with higher α excite a weak wakefield, reducing the maximum attainable energy. The maximum energy gain of the electrons is about 450 MeV for $\alpha = 0.5$, which is reasonably higher compared to the case of symmetric Gaussian pulses. These findings underscore the importance of pulse shaping in LWFA, demonstrating that modifying the temporal asymmetry of the laser pulse can serve as a powerful tool to enhance electron energy gain. The trends observed in the 2D simulations are further confirmed by the 3D PIC results, which show a consistent increase in the maximum electron energy with increasing pulse asymmetry (see Figure S1 in Supplementary Information).

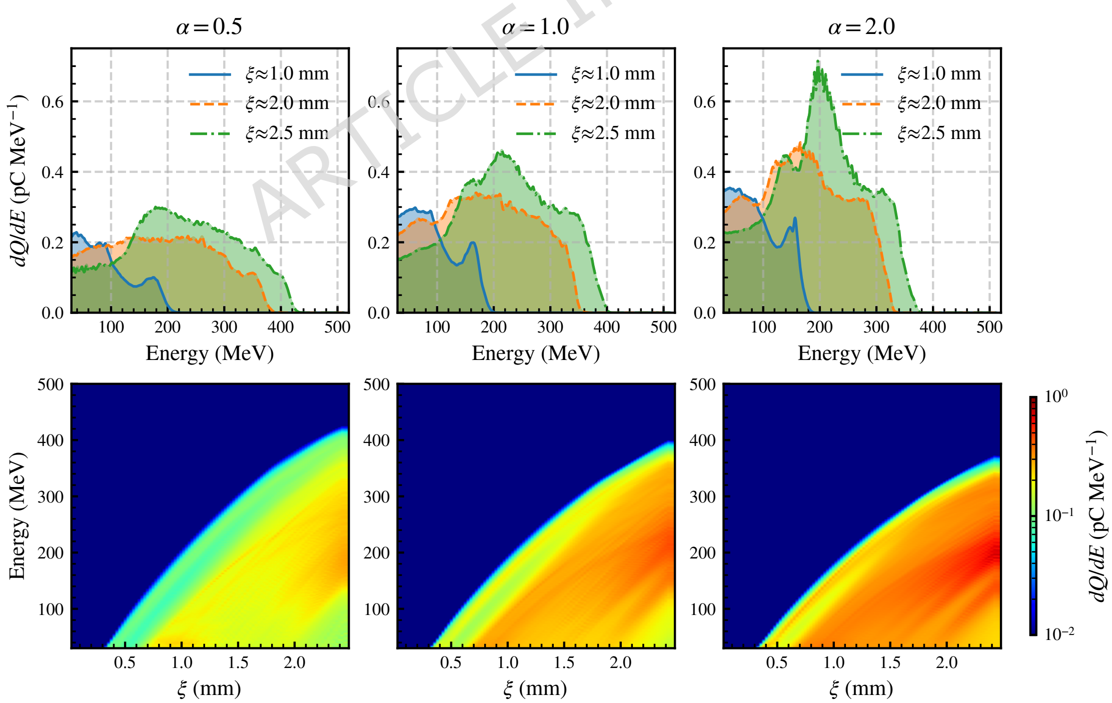

Figure 3. Electron charge distributions dQ/dE (in pC/MeV) for different values of α (0.5, 1.0, and 2.0) and at various propagation distances ($\xi \approx 1.0$ mm, 2.0 mm, and 2.5 mm). 2D-PIC results show the evolution of the charge spectrum as electrons propagate, with notable differences in spectral shapes and peak positions for different values of α and propagation lengths. In the bottom row, the corresponding spectrograms show the spatial evolution of the electron energy distribution.

While pulse-front steepening, group-velocity dispersion, self-phase modulation, and longitudinal reshaping can in general modify the laser temporal profile and relax the imposed asymmetry[31,32], we restrict our analysis to propagation distances shorter than the depletion and dispersion lengths and to moderate asymmetry parameters, for which prior studies have shown that the envelope structure is largely preserved over the relevant injection region.

Figure 3 illustrates the evolution of electron charge spectra (dQ/dE) resulting from ionization injection driven by an asymmetric laser pulse. For a higher degree of asymmetry ($\alpha = 2.0$), more efficient ionization and injection occur, producing a less energetic spectrum with a peak near 220 MeV and increased beam charge. In contrast, $\alpha = 0.5$ results in fewer trapped electrons and higher final energies, indicative of weaker ionization fields and reduced injection efficiency. With increasing propagation distances ($\xi \approx 1.0$ mm to 2.5 mm), the continuous rightward shift of the spectra reveals sustained acceleration of the injected electrons. Interestingly, higher values of α ($\alpha = 2.0$) lead to a more pronounced injection, evidenced by a higher spectral density and an increased total beam charge. However, the maximum and average electron energies are higher for $\alpha = 0.5$. This suggests that although more electrons are trapped and accelerated at higher α, beam loading and phase-space crowding may limit the energy gain per particle. At lower α, fewer electrons are injected, but they experience stronger or less saturated accelerating fields, allowing them to reach higher energies. The spectrograms in the bottom row confirm this aspect. For lower α, a more energetic bunch emerges, while for higher α, a denser but lower energy distribution forms. The case of symmetric pulses $\alpha = 1.0$ shows moderate injection and acceleration characteristics. Furthermore, the 3D PIC simulations corroborate these observations, demonstrating similar injection dynamics and energy scaling as shown in Figure S2 of the Supplementary Information.

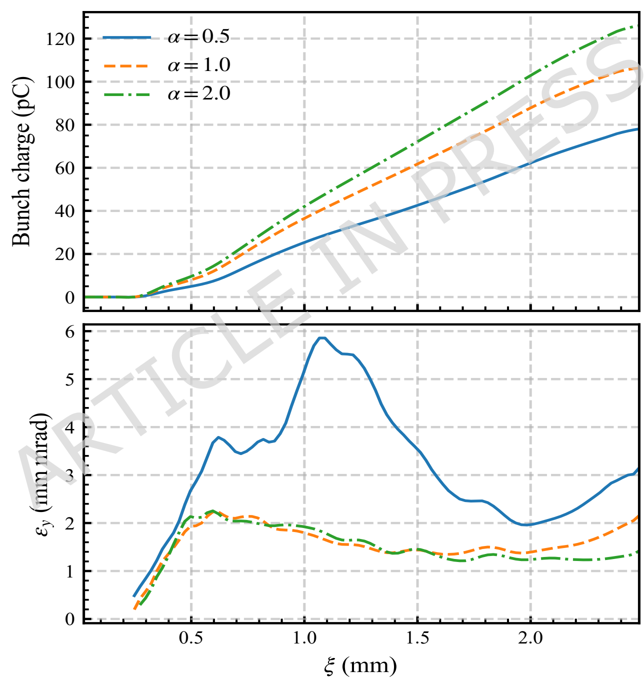

Figure 4. Evolution of beam properties for different temporal asymmetry parameters α. **(Top)** Total injected charge for $\alpha = 2.0$, 1.0, and 0.5, showing that higher asymmetry ($\alpha = 2.0$) results in greater charge injection. **(Bottom)** Corresponding evolution of the transverse rms emittance ε_y of the injected electron beam.

The results in Figure 4 demonstrate the effect of laser pulse asymmetry on ionization injection and its impact on electron bunch characteristics in LWFA. At higher asymmetry ($\alpha = 2.0$), a rapid increase in field strength leads to stronger ionization of nitrogen gas in the pulse field. This causes more electrons to be injected into the wake, significantly increasing the beam charge. The upper row of the figure indicates that a temporally asymmetric pulse with a larger α produces a higher-charge electron bunch with a trend toward reduced emittance in 2D PIC simulations, whereas a pulse with a smaller α yields a lower-charge bunch with a trend toward increased emittance. This effect is primarily attributed to the direct interaction between the injected electron bunch and the asymmetric laser pulse. Hence, laser asymmetry not only governs the charge and injection timing but also impacts transverse emittance through its interaction with the evolving electron bunch. The corresponding 3D PIC simulations shown in Figure S3 (see Supplementary Information) confirm these trends, showing consistent bunch characteristics.

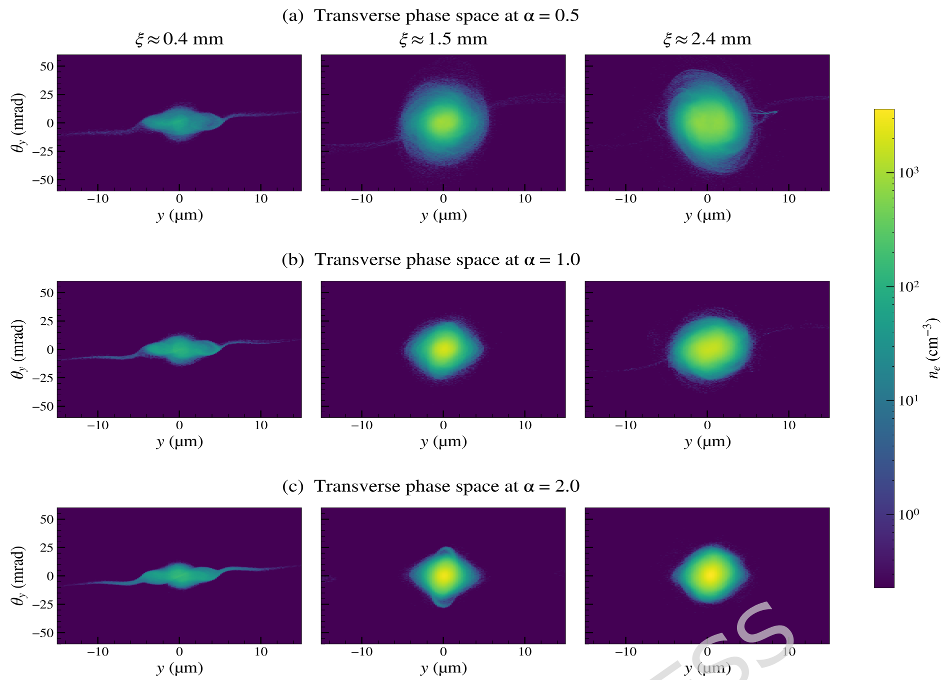

Figure 5. Transverse phase space (y, θ_y) evolution of the injected electron bunches at three different propagation distances (from left to right: $\xi = 0.4$ mm, $\xi = 1.5$ mm, and $\xi = 2.4$ mm, for three different laser asymmetry parameters (a) $\alpha = 0.5$, (b) $\alpha = 1.0$, and (c) $\alpha = 2.0$. The snapshots illustrate the effect of laser pulse asymmetry on the transverse emittance growth.

Figure 5 shows the evolution of the transverse phase-space (y, θ_y) of injected electrons at three key propagation distances for different pulse asymmetry $\alpha = 0.5, 1.0, 2.0$. The phase space distribution reveals critical insights into the beam transverse dynamics, including emittance growth and collimation. At early times ($\xi = 0.4$ mm), all beams are tightly confined near the origin, indicating the initial stage of injection. As propagation proceeds, with ξ values of 1.5 mm and 2.4 mm, noticeable differences begin to emerge. For the higher asymmetry ($\alpha = 2.0$), the rapid rising edge of the laser pulse ionizes and injects a large number of electrons in a short time. This leads to a denser bunch with a narrower spread in transverse phase-space (θ_y) due to strong space-charge forces during early and more localized injection. The small phase-space area implies a trend towards reduced transverse emittance. On the other hand, the low-asymmetry case ($\alpha = 0.5$) shows a broader distribution throughout propagation. Figure S5 of the Supplementary Information shows that the 3D PIC simulation results further substantiate these outcomes and are in good agreement.

Figure 6 compares the plasma electron density and the transverse electric field E_y for two different laser asymmetry parameters: $\alpha = 0.5$ and $\alpha = 2.0$. For $\alpha = 2.0$, the wakefield structure is more symmetric and well-formed, indicating a stable and focused plasma bubble. For the parameter range considered here, the overall bubble size and average cavity radius remain essentially unchanged, since they are mainly determined by the peak normalized vector potential , plasma density, and laser spot size. However, the pulse asymmetry does affect the local structure of the wake potential near the rear of the bubble. In particular, fast trailing pulses generate a sharper longitudinal field gradient at the back of the cavity, which leads to a transient steepening of the wake potential and a more localized injection region. This may be interpreted as a slight and temporary modification of the bubble shape near the rear, but without a significant change in the global bubble length or radius during propagation. This structure supports a stronger and more coherent longitudinal accelerating field behind the laser pulse, which favors the forward-directed acceleration of the electron bunch with reduced transverse spread. On the other hand, for slow trailing pulses, the plasma wake appears more distorted, with a less uniform structure. This irregularity weakens the effective accelerating field and may introduce transverse forces that can deflect the bunch or reduce its collimation. Consequently, the directionality and efficiency of bunch acceleration are enhanced at higher asymmetry values, where the wakefield structure better supports forward propagation of the electron bunch. In summary, the choice of laser asymmetry parameter α presents a trade-off: low α yields higher energy via stronger wakefields, while high α produces a trend towards lower emittance due to reduced laser-electron coupling. The optimal choice depends on the specific requirements for energy versus beam quality in a given application.

To understand the quality of the bunch, in Figure 7, we depicted the average charge distribution of the electron bunch

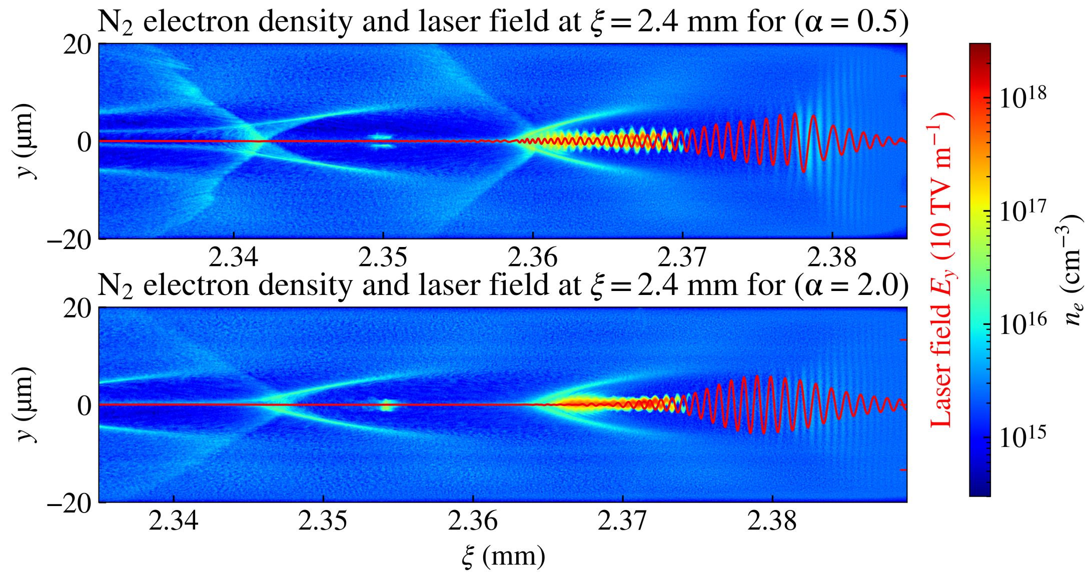

Figure 6. Snapshots of the normalized electron density n_e (in cm^{-3}) and transverse electric field E_y (in units of 10 TV/m) at $\xi = 2.4$ mm for asymmetry parameters: (top) $\alpha = 0.5$ and (bottom) $\alpha = 2.0$.

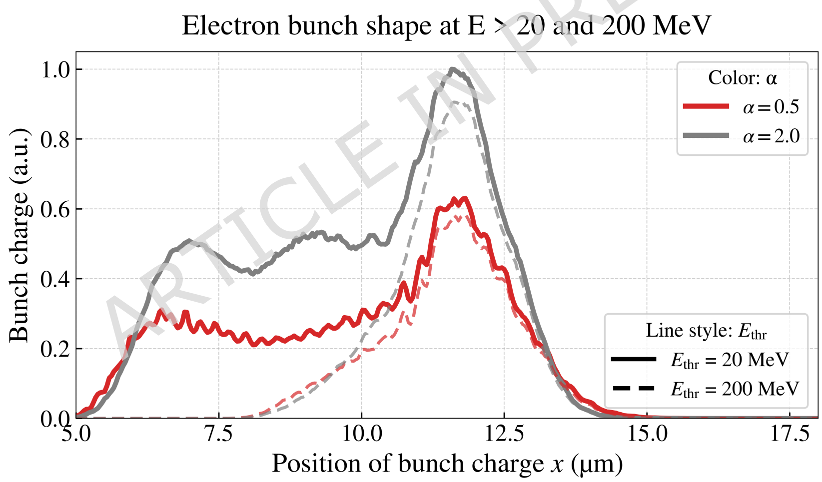

Figure 7. Electron bunch charge distribution along the propagation direction ξ for laser pulse asymmetry parameters ($\alpha = 0.5$, red; $\alpha = 2.0$, gray), shown for electrons with energies exceeding $E_{\text{thr}} = 20\,\text{MeV}$ (solid lines) and $200\,\text{MeV}$ (dashed lines). The bunch of the injected electrons under different pulse asymmetry conditions is shown, highlighting more compact and energetic bunch formation in the fast-rise ($\alpha = 0.5$) case.

($E > 20MeV$) around the propagation distance of 2400 μm for $\alpha = 0.5$ (red curve) and $\alpha = 2.0$ (black curve). For $\alpha = 0.5$, the bunch charge is less, indicating a brief and localized injection phase. For $\alpha = 2.0$, the bunch is longer, with multiple peaks and an extended tail, suggesting prolonged injection and potential multi-bunch formation. The trends observed in the 2D simulations are also evident in the 3D PIC results, which show the formation of multiple electron bunches (see Figure S5 in the Supplementary Information). However, we emphasize that the present diagnostics provide only an indirect estimate of the temporal duration of the injected bunches. Therefore, the observed charge modulation should be interpreted as evidence of the potential for ultrashort bunch formation rather than as definitive confirmation of attosecond-scale bunches. Further investigation using higher-resolution diagnostics and complementary methods is necessary to establish the exact temporal characteristics of the electron bunches.

Theoretical Model

The Hamiltonian for an electron in wakefield (ϕ) excited by the asymmetric pulse can be written as[33]

$$H(\xi, p) = \sqrt{1+p^2} - \beta_p p + \frac{1}{2}\omega_p^2\xi^2 - B\xi^3, \tag{1}$$

where $p = p_\xi/m_e c$, $\beta_p = v_p/c = 1 \approx 1 - 1/2\gamma_p^2$, γ_p is the Lorentz factor of the wakefield, ϕ is normalized by $m_e c^2/e$, $\gamma = \sqrt{1+p^2}$, and $\xi = z - v_\phi t$ is the co-moving coordinate, $p_\xi = \gamma m_e v_\xi$ is the canonical momentum, $\omega_p = \sqrt{4\pi n_e e^2/m_e}$ is the electron plasma frequency, m_e is the electron mass, and e is the electron charge. Here, $B = B_0 a_0^2(\frac{1}{t_r^3} - \frac{1}{t_f^3})$ gives the asymmetricity of the laser pulse, where $B_0 = \frac{e^3 n_0}{12\varepsilon_0 m_e^2 c^2 \omega_0^2}$, n_0 is the plasma electron density, ε_0 is the vacuum permitivity, ω_0 is the laser frequency, and c is the velocity of light in vacuum. B will be zero for the symmetric Gaussian pulse.
Using Hamiltonian, the equation of motion can be written as[13,34]

$$\frac{d\xi}{dt} = \frac{dH}{d\phi} = \frac{p}{\sqrt{1+p^2}} - \beta_p, \tag{2}$$

$$\frac{dp}{dt} = -\frac{dH}{d\xi} = -\omega_p^2 + 3B\xi^2. \tag{3}$$

A temporally asymmetric laser pulse modifies the coefficients B and ω_p^2 dynamically, and can also shift β_p. For a fast trailing edge, B increases transiently, modifying the separatrix. This lowers the effective trapping threshold and promotes electron injection. On the other hand, a slow trailing pulse produces a smoother wake (smaller B), reducing asymmetry and suppressing trapping. Thus, pulse asymmetry provides a direct control on the dynamics of separatrix motion and the optimization of electron injection in laser wakefield acceleration.
In the ionization injection scheme of LWFA, the ionized electrons are usually born at rest (i.e. $p = 0$) and the Hamiltonian is $H_0 = 1 + \frac{1}{2}\omega_p^2\xi_0^2 - B\xi_0^3$, where $\xi = \xi_0$ is the position inside the wake.
In pure hydrogen, plasma electrons come only from fully ionized H (1 electron per atom). In a hydrogen-nitrogen mixture, additional high Z electrons (e.g. from N^{5+} to N^{7+}) are ionized within the wake. The rising and falling edges of the laser have different intensities, which create an asymmetric ponderomotive force. The asymmetry term $B\xi^3$ makes the rear of the wake deeper, increasing trapping efficiency.
For the injection of electrons, the injection energy is controlled by the injection timing. If an asymmetric pulse ionizes electrons near the peak or in the trailing part, they experience a strong wakefield and are more likely to be trapped. Using the Hamiltonian given above, we write

$$\gamma_\parallel = 1 + \frac{e}{m_e c^2}\left(\frac{1}{2}\omega_p^2\xi^2 - B\xi^3\right). \tag{4}$$

For trapping

$$1 + \frac{e}{m_e c^2}\left(\frac{1}{2}\omega_p^2\xi^2 - B\xi^3\right) + \left(1 + \frac{a_0^2}{2}\right) \geq \gamma_p. \tag{5}$$

This means that the laser pulse shape parameter influences the electron injection, which can be understood by using the Hamiltonian phase-space trajectories of electrons for symmetric and asymmetric pulses. The electrons are trapped in the wake if $\gamma_\perp + \gamma_\parallel \geq \gamma_p$, where $\gamma_\perp = 1 + a_0^2/2$, $\gamma_\parallel$ is the longitudinal energy gain.
One needs to define the separatrix to understand the trapped and untrapped electrons. A separatrix is the boundary in phase-space that separates trapped and untrapped electrons. Its Hamiltonian represents the momentum–energy balance of released electrons, which determines whether they can be trapped and accelerated in the plasma wake[33,34]. For a relativistic wakefield, the separatrix Hamiltonian is $H_S = \gamma_\phi - \phi_{min}$, where $\gamma_\phi = (1-\beta_\phi^2)^{-1/2}$ and ϕ_{min} is the minimum wakefield potential. Using $\phi = -\frac{1}{2}\omega_p^2\xi^2 - B\xi^3$, for minima, we get $\frac{d\phi}{d\xi} = \omega_p^2\xi + 3B\xi^2 = 0$, which gives two positions for minima, that is, $\xi = 0$ and $\xi = -\omega_p^2/3B$. At the non-zero point ($\xi = -\omega_p^2/3B$), $\phi_{min} = -\omega_p^6/54B^2$. This gives the separatrix Hamiltonian

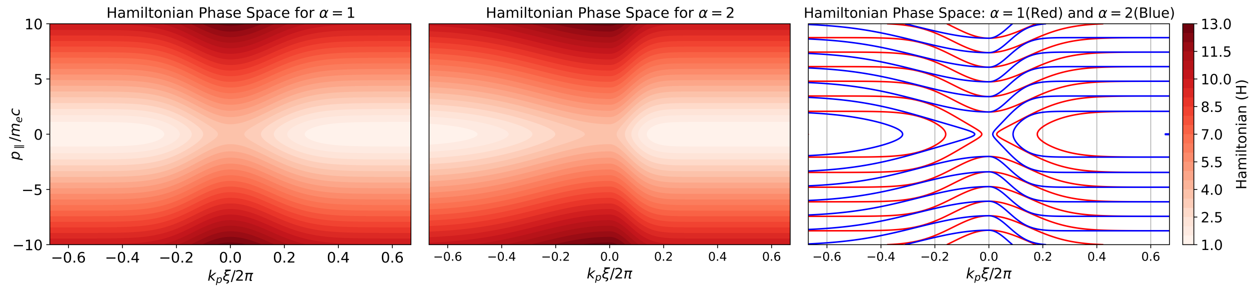

Figure 8. Hamiltonian phase-space contours $H(\xi, p_\parallel)$ for symmetric ($\alpha = 1.0$), asymmetric ($\alpha = 2.0$) laser pulses and the corresponding phase-space trajectory for $\alpha = 1.0$ (red) and $\alpha = 2.0$ (blue), illustrating the influence of pulse asymmetry on electron dynamics in the co-moving coordinate $\xi = z - ct$. The laser has normalized vector potential $a_0 = 2.65$, spot size $w_0 = 10\ \mu$m, pulse duration $\tau_{\text{FWHM}} = 30$ fs, and wavelength $\lambda = 0.8\ \mu$m, propagating in plasma with density $n_0 = 5\times 10^{18}$ cm^{-3}. The presence of 0.5% nitrogen gas in the plasma introduces inner-shell electrons from ionization of N^{5+} to N^{7+}.

$H_S = \gamma_\phi + \omega_p^6/54B^2$. One may see that the trapped region will be enlarged for pulse asymmetry. The potential well is deeper, and the separatrix is wider and higher, allowing more electrons (from N inner shells) to be trapped.
To compare the parallel momentum ($\gamma_\parallel$) and injection threshold for pure hydrogen vs hydrogen + 0.5% nitrogen, for interaction with asymmetric laser pulses, one needs to analyze how the injection condition changes. Pure Hydrogen (with symmetric pulse), the wakefield potential is symmetric with a shallower wake potential. The electrons ionized from hydrogen near the front of the wake, with relatively small ξ. Thus $\gamma_\parallel$ is limited, and a higher injection threshold can be seen due to a small wake depth. On the other hand, for hydrogen + 0.5% nitrogen interaction with an asymmetric pulse, the wake has asymmetricity, a deeper potential well at larger ξ. Electrons from inner shells of nitrogen (e.g. $N^{5+} \to N^{7+}$) are ionized late, near the back of the wake, where ξ is large. Thus, the parallel momentum ($\gamma_\parallel$) is subsequently large, which enhances the wake depth and reduces the injection threshold. Overall, the injection probability is enhanced for an asymmetric laser pulse in hydrogen gas mixed with nitrogen gas.
Figure 8 represents Hamiltonian phase-space contours $H(\xi, p_\parallel)$ for electrons interacting with symmetric and asymmetric laser pulses, highlighting how pulse asymmetry influences electron dynamics and potential trapping. The co-moving coordinate is defined as $\xi = z - ct$, with normalized momentum $p_\parallel/m_ec$ plotted against the normalized spatial coordinate $k_p\xi/2\pi$. These results clearly show that, for a symmetric laser pulse ($\alpha = 1.0$), the Hamiltonian contours exhibit a regular, symmetric structure in phase space. The potential well is relatively uniform, leading to more predictable electron trajectories. Instead, with an asymmetric pulse ($\alpha = 2.0$), the Hamiltonian phase space becomes distinctly skewed. The asymmetry in the laser envelope, characterized by a sharper rise and slower fall time or vice versa, reshapes the contours and modifies potential trapping regions. This skewing enhances the likelihood of ionized electrons being captured into favorable regions of the wakefield, thereby increasing trapping efficiency. The phase-space trajectories for both $\alpha = 1.0$ and $\alpha = 2.0$ further illustrate how the asymmetry directly alters the dynamics of injected electrons, with the blue trajectory (for $\alpha = 2.0$) showing deeper penetration into trapping regions compared to the red trajectory (for $\alpha = 1.0$). Thus, electron trapping and injection in plasma-based accelerators can be effectively controlled by tailoring the laser pulse shape in ionization injection regime utilizing high Z dopants such as nitrogen.

Methodological Limitations and Extension to 3D

While 2D-PIC simulations provided physical insight and enable extensive parameter scans at manageable computational cost, they are inherently limited in their ability to capture the full complexity of beam emittance, which is a fundamentally 3D process. One key limitation of 2D geometry is the artificial confinement of the laser pulse and plasma wake in the out-of-plane direction. In 2D Cartesian simulations, the laser effectively propagates as a sheet-like beam, which modifies diffraction, self-focusing, and energy depletion compared to a true 3D Gaussian beam. This can lead to quantitative differences in the evolution of the bubble radius, the wake phase velocity, and the injection threshold. As a result, absolute values of beam parameters such as emittance, charge, and energy spread obtained in 2D are not expected to be quantitatively accurate when extrapolated to 3D. In addition, collective beam-loading effects are fundamentally altered in 2D, where the space-charge fields of the accelerated bunch scale differently with charge density in 3D. In 2D, only a single transverse degree of freedom is available, which artificially constrains betatron motion and suppresses phase-space decoherence mechanisms that are present in 3D. Consequently, normalized transverse emittances and projected energy spreads extracted from 2D simulations tend to be systematically lower than their 3D counterparts.

Despite these limitations, the primary objective of the present 2D study is to identify qualitative trends and underlying physical mechanisms governing the role of laser pulse temporal asymmetry in ionization-induced injection. In particular, the suppression of prolonged injection and the resulting improvement in beam quality with increasing asymmetry parameter α are robust features of the wakefield evolution and are not inherently tied to the dimensionality of the simulation. To partially address the above concerns and assess the robustness of the 2D trends, we have performed a limited set of quasi-3D PIC simulations for all three representative values of the temporal asymmetry parameter. These preliminary 3D results, reported in Supplementary Information S1, include the normalized transverse emittance ε_n as well as the relative energy spread for both cases. While the absolute beam quality metrics differ from their 2D counterparts, the qualitative trend—namely, improved beam quality and reduced injection duration for larger α is preserved in three dimensions.

Conclusions

In this work, we have investigated the influence of laser pulse asymmetry, governed by the parameter α, on the ionization injection regime of LWFA. By systematically varying the temporal asymmetry of the laser pulse while maintaining constant FWHM of the laser pulse, we explored its effects on wakefield generation, injection dynamics, beam energy, and emittance. Our 2D-PIC results revealed that fast trailing pulses ($\alpha = 0.5$) induces stronger ponderomotive forces, leading to the generation of more intense wakefields. This promotes early and efficient injection of ionization from nitrogen dopants and results in significantly higher electron energies. However, because of the more localized and weaker injection volume, the total injected charge is reduced. However, slow trailing pulses ($\alpha = 2.0$) leads to a stronger overlap between the laser field and the injection region, producing a higher beam charge through denser electron injection. However, the increased beam loading limits the available accelerating field, resulting in lower final electron energies. Importantly, the reduced direct interaction between the laser and the injected electrons in this case also suppresses transverse momentum growth, yielding lower transverse emittance and improved beam collimation.

In conclusion, our study demonstrated that laser pulse asymmetry can serve as an effective parameter for controlling the LWFA performance in ionization injection regime. A lower α favors high-energy applications, while a higher α benefits scenarios requiring lower emittance and a higher charge. These findings underline the critical importance of temporal pulse shaping in tailoring electron beam properties for specific experimental and application-driven requirements in advanced accelerator technologies.

Methods

To investigate the influence of laser pulse asymmetry on electron acceleration in ionization injection regime of LWFA, we performed 2D-PIC simulations using the EPOCH framework[35]. The simulations model the propagation of an intense laser pulse through a mixed gas target consisting of hydrogen mixed with 0.5% nitrogen, capturing the evolution of the wakefield structure and the dynamics of injected electrons. The laser pulse is linearly polarized and Gaussian, with a normalized vector potential of $a_0 = 2.65$, a spot size $r_0 = 10\ \mu$m, FWHM pulse duration $\tau_{\text{FWHM}} = 30$ fs, and a central wavelength of $\lambda = 0.8\ \mu$m. The laser propagates along the z direction in a pre-ionized plasma with electron density $n_0 = 5\times10^{18}$ cm^{-3}. To study the effect of temporal pulse asymmetry, we model different temporal profiles characterized by the asymmetry parameter (α), while maintaining the same FWHM duration. The laser pulse ionizes hydrogen gas to form a background plasma. This can occur at laser intensity $I_0 = 10^{14} W/cm^2$, producing fast electrons to contribute to wakefield generation. Ionization of inner-shell electrons from N^{5+} to N^{7+} is modelled using the ADK tunnel ionization rate. This facilitates the injection of electrons into the wakefield due to the high ionization threshold of the inner-shell electrons and their release in the strong laser field region. For both gases, we used the ADK model of ionization. Following the ADK model of ionization[36], the ionization rate $\Gamma(t)_{H,N_2}$ can be given as

$$\Gamma(t)_{H,N_2} = \Gamma_{0H,0N_2} I(t)_L^{3/2} \exp\left(-\frac{\gamma_{H,N_2}}{I(t)_L}\right), \tag{6}$$

where $I(t)_L$ is the laser intensity at time t, $\Gamma_{0H,0N_2}$ is a constant that depends on the ionization potential of hydrogen and nitrogen gas, γ_{H,N_2} is a constant that characterizes the ionization threshold for hydrogen and nitrogen gas.

The evolution of the electron density n_e in the plasma is governed by the continuity equation

$$\frac{\partial n_e}{\partial t} + \nabla . n\mathbf{v} = n_g \Gamma(t)_{H,N_2}, \tag{7}$$

where n_g is the gas density of the mixture of hydrogen and nitrogen gas and n_e is the plasma electron density. The term $n_g\Gamma(t)_{H,N_2}$ accounts for the number of electrons ionized per unit time due to the laser field.

References

1. Tajima, T. & Dawson, J. Laser electron accelerator. *Phys. Rev. Lett.* **43**, 267–270, DOI: 10.1103/PhysRevLett.43.267 (1979).
2. Brunetti, E. *et al.* Low emittance, high brilliance relativistic electron beams from a laser-plasma accelerator. *Phys. Rev. Lett.* **105**, 215007, DOI: https://doi.org/10.1103/PhysRevLett.105.215007 (2010).
3. Faure, J. *et al.* A laser-plasma accelerator producing monoenergetic electron beams. *Nature* **431**, 541–544, DOI: https://doi.org/10.1038/nature02963 (2004).
4. Mangles, S. P. *et al.* Monoenergetic beams of relativistic electrons from intense laser-plasma interactions. *Nature* **431**, 535–538, DOI: https://doi.org/10.1038/nature02939 (2004).
5. Geddes, C. *et al.* High-quality electron beams from a laser wakefield accelerator using plasma-channel guiding. *Nature* **431**, 538–541, DOI: https://doi.org/10.1038/nature02900 (2004).
6. Wiggins, S. *et al.* High quality electron beams from a laser wakefield accelerator. *Plasma Phys. Control. Fusion* **52**, 124032, DOI: https://doi.org/10.1088/0741-3335/52/12/124032 (2010).
7. Malka, V. Laser plasma accelerators. *Phys. Plasmas* **19**, 055501, DOI: https://doi.org/10.1063/1.3695389 (2012).
8. Gonsalves, A. J. *et al.* Petawatt laser guiding and electron beam acceleration to 8 gev in a laser-heated capillary discharge waveguide. *Phys. Rev. Lett.* **122**, 084801, DOI: https://doi.org/10.1103/PhysRevLett.122.084801 (2019).
9. Döpp, A. *et al.* Energy boost in laser wakefield accelerators using sharp density transitions. *Phys. Plasmas* **23**, 056702, DOI: https://doi.org/10.1063/1.4946018 (2016).
10. Gupta, D. N., Yadav, M., Jain, A. & Kumar, S. Electron bunch charge enhancement in laser wakefield acceleration using a flattened gaussian laser pulse. *Phys. Lett. A* **414**, 127631, DOI: https://doi.org/10.1016/j.physleta.2021.127631 (2021).
11. Jain, A. *et al.* The effect of laser pulse evolution on down-ramp injection in laser wakefield accelerators. *Sci. Reports* **14**, 19127, DOI: https://doi.org/10.1038/s41598-024-69049-4 (2024).
12. Suk, H., Barov, N., Rosenzweig, J. B. & Esarey, E. Plasma electron trapping and acceleration in a plasma wake field using a density transition. *Phys. Rev. Lett.* **86**, 1011–1014, DOI: https://doi.org/10.1103/PhysRevLett.86.1011 (2001).
13. Pak, A. *et al.* Injection and trapping of tunnel-ionized electrons into laser-produced wakes. *Phys. Rev. Lett.* **104**, 025003, DOI: https://doi.org/10.1103/PhysRevLett.104.025003 (2010).
14. McGuffey, C. *et al.* Ionization induced trapping in a laser wakefield accelerator. *Phys. Rev. Lett.* **104**, 025004, DOI: https://doi.org/10.1103/PhysRevLett.104.025004 (2010).
15. Schmid, K. *et al.* Density-transition based electron injector for laser driven wakefield accelerators. *Phys. Rev. ST Accel. Beams* **13**, 091301, DOI: https://doi.org/10.1103/PhysRevSTAB.13.091301 (2010).
16. Tsai, H. E. *et al.* Control of quasi-monoenergetic electron beams from laser-plasma accelerators with adjustable shock density profile. *Phys. Plasmas* **25**, DOI: https://doi.org/10.1063/1.5023694 (2018).
17. Tooley, M. P. *et al.* Towards attosecond high-energy electron bunches: Controlling self-injection in laser-wakefield accelerators through plasma-density modulation. *Phys. Rev. Lett.* **119**, 044801, DOI: https://doi.org/10.1103/PhysRevLett.119.044801 (2017).
18. Jain, A. & Gupta, D. N. Optimization of electron bunch quality using a chirped laser pulse in laser wakefield acceleration. *Phys. Rev. Accel. Beams* **24**, 111302, DOI: https://doi.org/10.1103/PhysRevAccelBeams.24.111302 (2021).
19. Chen, M., Esarey, E., Schroeder, C. B., Geddes, C. G. R. & Leemans, W. P. Theory of ionization-induced trapping in laser-plasma accelerators. *Phys. Plasmas* **19**, 033101, DOI: 10.1063/1.3689922 (2012).
20. Jain, A. & Gupta, D. N. Improvement of electron beam quality in laser wakefield acceleration by a circularly-polarized laser pulse. *Plasma Phys. Control. Fusion* **63**, 075007, DOI: https://doi.org/10.1088/1361-6587/abfd7d (2021).
21. Gu, Y. *et al.* Generation of highly stable electron beam via the control of hydrodynamic instability. *Sci. Reports* **14**, DOI: https://doi.org/10.1038/s41598-024-82304-y (2024).
22. Picksley, A. *et al.* All-optical gev electron bunch generation in a laser-plasma accelerator via truncated-channel injection. *Phys. Rev. Lett.* **131**, 245001, DOI: https://doi.org/10.1103/PhysRevLett.131.245001 (2023).
23. Gupta, D. N., Yoffe, S. R., Jain, A., Ersfeld, B. & Jaroszynski, D. A. Propagation of intense laser pulses in plasma with a prepared phase-space distribution. *Sci. Reports* **12**, DOI: https://doi.org/10.1038/s41598-022-24664-x (2022).

24. Hue, C. S., Wan, Y., Levine, E. Y. & Malka, V. Control of electron beam current, charge, and energy spread using density downramp injection in laser wakefield accelerators. *Matter Radiat. at Extrem.* **8**, 024401, DOI: https://doi.org/10.1063/5.0126293 (2023).

25. Leemans, W. P. *et al.* Electron-yield enhancement in a laser-wakefield accelerator driven by asymmetric laser pulses. *Phys. Rev. Lett.* **89**, 174802, DOI: https://doi.org/10.1103/PhysRevLett.89.174802 (2002).

26. Gopal, K. & Gupta, D. N. Optimization and control of electron beams from laser wakefield accelerations using asymmetric laser pulses. *Phys. Plasmas* **24**, 103101, DOI: https://doi.org/10.1063/1.5001849 (2017).

27. Parize, G. *et al.* Temporal pulse shaping technique for nonlinear frequency shifting. *Appl. Phys. Lett.* **126**, 101105, DOI: 10.1063/5.0254035 (2025).

28. Jaroszynski, D. A. & Vieux, G. Coherent radiation sources based on laser plasma accelerators. *AIP Conf. Proc.* **647**, 902–914, DOI: https://doi.org/10.1063/1.1524946 (2002).

29. Cipiccia, S. *et al.* Gamma-rays from harmonically resonant betatron oscillations in a plasma wake. *Nat. Phys.* **7**, DOI: https://doi.org/10.1038/nphys2090 (2011).

30. Polanek, R. *et al.* 1 khz laser accelerated electron beam feasible for radiotherapy uses: A pic–monte carlo based study. *Nucl. Instruments Methods Phys. Res. Sect. A: Accel. Spectrometers, Detect. Assoc. Equip.* **987**, 164841, DOI: https://doi.org/10.1016/j.nima.2020.164841 (2021).

31. Benedetti, C., Rossi, F., Schroeder, C. B., Esarey, E. & Leemans, W. P. Pulse evolution and plasma-wave phase velocity in channel-guided laser-plasma accelerators. *Phys. Rev. E* **92**, 023109, DOI: 10.1103/PhysRevE.92.023109 (2015).

32. Esarey, E., Schroeder, C. B. & Leemans, W. P. Physics of laser-driven plasma-based electron accelerators. *Rev. Mod. Phys.* **81**, 1229–1285, DOI: 10.1103/RevModPhys.81.1229 (2009).

33. Esarey, E. & Pilloff, M. Trapping and acceleration in nonlinear plasma waves. *Phys. Plasmas* **2**, 1432–1436, DOI: 10.1063/1.871358 (1995).

34. Kalmykov, S., Yi, S. A., Khudik, V. & Shvets, G. Electron self-injection and trapping into an evolving plasma bubble. *Phys. Rev. Lett.* **103**, 135004, DOI: 10.1103/PhysRevLett.103.135004 (2009).

35. Arber, T. D. *et al.* Contemporary particle-in-cell approach to laser-plasma modelling. *Plasma Phys. Control. Fusion* **57**, 113001, DOI: https://doi.org/10.1088/0741-3335/57/11/113001 (2015).

36. Keldysh, L. V. Ionization in the field of a strong electromagnetic wave. *Sov. Phys. JETP* **20**, 1307 (1965).

Data availability

The data supporting the findings of this study are available upon reasonable request from the corresponding author.

Funding

This work was financially supported by the Science and Engineering Research Board (now Anusandhan National Research Foundation), Government of India (Grant No. CRG/2022/001989) and the National Research Foundation of Korea under Grant No. RS-2022-NR070637.

Author contributions

The project was conceived by Ravina and DNG. Simulations were performed by Ravina and SK. Discussion, analysis, interpretation, writing and validation was undertaken by Ravina, SK, DNG, and HS.

Competing interests

The authors declare no competing interests.